

Crystal size and magnetic field effects in Co_3O_4 antiferromagnetic nanocrystals

T. Mousavand,¹ T. Naka,^{1,2,*} K. Sato,¹ S. Ohara,¹ M. Umetsu,¹ S. Takami,¹ T. Nakane,² A. Matsushita,² and T. Adschiri³

¹*Institute of Multidisciplinary Research for Advanced Materials, Tohoku University, 2-1-1 Katahira, Aoba-ku, Sendai 980-8577, Japan*

²*National Institute for Materials Science, 2-1-1 Sengen, Tsukuba, Ibaraki 305-0047, Japan*

³*WPI, Advanced Institute for Materials Research, Tohoku University, 2-1-1 Katahira, Aoba-ku, Sendai 980-8577, Japan*

(Received 26 December 2008; revised manuscript received 15 March 2009; published 13 April 2009)

We report magnetism of spinel Co_3O_4 nanocrystals with average diameters of ~ 25 and ~ 100 nm under magnetic fields up to 50 kOe. The nanoparticles were controlled to be cubic in shape. In the smaller nanocrystal sample ($d \sim 25$ nm), a spontaneous magnetic moment increased steeply below the Néel point, $T_N = 32$ K of the bulk sample, whereas similar to bulk samples the larger crystal sample ($d \sim 100$ nm) exhibited a maximum in magnetization around T_N . A spin-glass-like behavior in magnetization was observed at $T_i = 10$ K at lower magnetic fields, whereas above $H = 30$ kOe, this behavior disappeared.

DOI: 10.1103/PhysRevB.79.144411

PACS number(s): 75.75.+a, 61.46.Df, 73.63.Bd

I. INTRODUCTION

As the crystal size approaches the nanometer scale, the intrinsic properties of individual particles and dominant magnetic interactions are distinguishable from those of the respective bulk materials. For ferromagnetic and ferrimagnetic materials, the effects of crystal size and of exposed crystallographic surfaces on magnetism have been investigated intensively.^{1,2} In contrast, comprehensive experimental investigations of antiferromagnetism in nanoscale materials have not been undertaken, although anomalous magnetism has been predicted theoretically in antiferromagnetic nanocrystals.^{2,3} Here, we report the size and magnetic field effects on magnetism in antiferromagnetic cobalt oxide (Co_3O_4) nanocrystals synthesized under hydrothermal conditions with cubic or rectangular solid shapes. By using a hydrothermal synthesis method with organic ligands as surface modifiers, we can control the crystal size and morphology of the obtained fine particles.⁴⁻⁷ Therefore, compared with particles synthesized by mechanical milling⁸ methods or by deposition into a matrix,⁹ our crystals appear to have high crystallinity. Co_3O_4 has a normal spinel structure of which the ionic (valence) configuration can be expressed as $(\text{Co}^{2+})[\text{Co}^{3+}_2]\text{O}_4$, where (\cdots) and $[\cdots]$ represent the occupations at the tetrahedral A and the octahedral B sites, respectively. In the spinel structure, Co^{3+} ions in the octahedral sites (B sites) are in the low-spin state ($S=0$), and Co^{2+} ions on tetrahedral sites (A sites) have a spin of $3/2$. The spins on the A site form a collinear antiferromagnetic arrangement below $T_N \sim 30$ K.^{10,11} Generally, as the size of the particles decreases to nanometers, surface modifications and particle morphology strongly affect the core state of the crystals, including the valence and magnetic state.¹² The low transition temperature $T_N \sim 30$ K makes Co_3O_4 an ideal system to examine the size effects on magnetism in both the antiferromagnetic and the paramagnetic states while avoiding recrystallization at high temperatures that may occur in the case of NiO with $T_N = 523$ K. In this paper, we note that as the crystal size was reduced to a few tenths of a nanometer, the particles exhibited complicated magnetic behavior below the antiferromagnetic transition and also an increment of paramagnetic moment.

II. EXPERIMENTAL

Stainless steel (SUS 316) pressure-resistant tube reactors with an inner volume of 5.0 ml were used for hydrothermal synthesis. Each reactor was loaded with 2.5 ml of 0.1M $\text{Co}(\text{NO}_3)_2$. To obtain nanocrystalline samples of cobalt oxide, 0.2 ml of $\text{CH}_3(\text{CH}_2)_8\text{COOH}$ or $\text{CH}_3(\text{CH}_2)_9\text{NH}_2$ was added to the reactors. Each reactor was then capped tightly and put in an electric furnace that was maintained at 300 °C. The pressure inside the reactor was estimated to be 8.6 MPa during the reaction at 300 °C. The reaction was allowed to proceed for 10 min and terminated by submerging the reactor in a water bath. The products were removed from the reactors and were subjected to three cycles of washing with ethanol and centrifugation to remove the supernatant. The resulting purified nanocrystals were dried under vacuum overnight and then analyzed. The crystallographic identity of the synthesized nanoparticles was determined by a D/MAX γ_n x-ray diffractometer (XRD) (Rigaku) with $\text{Cu } K\alpha$ radiation. Particle sizes and lattice constants were estimated from a simulated XRD pattern obtained from CrystalDiffract software (CrystalMaker Software Ltd.). The size and morphology of the products were observed with a transmission electron microscope (TEM) (JEM-1200 EX II, JEOL). Magnetic measurements were carried out with a superconducting quantum interference device magnetometer [magnetic properties measurement system (MPMS), Quantum Design] under a magnetic field up to 50 kOe in the temperature range of 5–300 K. To prevent the crystals from rotating in the magnetic field, the samples were cast in paraffin.

III. RESULTS AND DISCUSSION

Figure 1(a) shows XRD patterns for cobalt oxide nanocrystals synthesized at 300 °C, with $\text{CH}_3(\text{CH}_2)_8\text{COOH}$ and $\text{CH}_3(\text{CH}_2)_9\text{NH}_2$ as modifier reagents. It was indicated by XRD measurements that a mixture of Co_3O_4 and CoO crystals was produced from cobalt nitrite at 300 °C (subcritical water) without any modifiers. However, when the crystals were synthesized by hydrothermal reactions with $\text{CH}_3(\text{CH}_2)_8\text{COOH}$ and $\text{CH}_3(\text{CH}_2)_9\text{NH}_2$ at 300 °C, single-

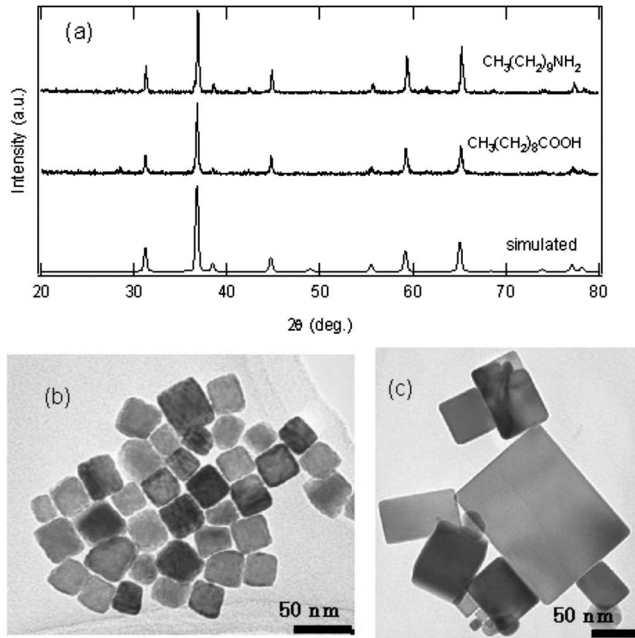


FIG. 1. (a) XRD patterns of cobalt oxide nanocrystals modified with $\text{CH}_3(\text{CH}_2)_8\text{COOH}$ and with $\text{CH}_3(\text{CH}_2)_9\text{NH}_2$ along with the simulated XRD pattern for spinel cobalt. [(b) and (c)] TEM images of (b) $\text{CH}_3(\text{CH}_2)_8\text{COOH}$ -modified and (c) $\text{CH}_3(\text{CH}_2)_9\text{NH}_2$ -modified Co_3O_4 nanocrystals.

phase Co_3O_4 was obtained. As shown in Fig. 1(a), all reflections of XRD patterns for both samples synthesized with the modifiers are assigned as the face-centered-cubic phase (spacing group $Fd\bar{3}m$) of spinel cobalt.¹³ The crystallographic data for the nanocrystal samples obtained in this study are listed in Table I. The XRD pattern simulation software was used to calculate the lattice constants and crystal sizes. The phase and morphology controls for oxide nanocrystals synthesized under subcritical hydrothermal condition have been reported elsewhere.⁴⁻⁷

Figure 1(b) shows the TEM images of the cobalt oxide nanocrystals synthesized with the modifiers shown in Fig. 1(a). For $\text{CH}_3(\text{CH}_2)_9\text{NH}_2$ -modified Co_3O_4 nanoparticles, the TEM image shows that these particles were 18–200 nm in size, with cubic and rectangular shapes [Fig. 1(c)]. In contrast, for the $\text{CH}_3(\text{CH}_2)_8\text{COOH}$ -modified sample [Fig. 1(b)], a homogenous cubic morphology of Co_3O_4 crystals with an average size of 25 nm was observed.

Figure 2 shows the magnetic susceptibility, $\chi(T) = M(T)/H$, as a function of temperature from $T=5$ to 65 K at $H=1$ kOe for particle diameters of $d=25$ and 92 nm. Below 32 K, the χ - T curve of $d=25$ nm is quite different from that of $d=92$ nm. For $d=25$ nm, the magnetic susceptibility in-

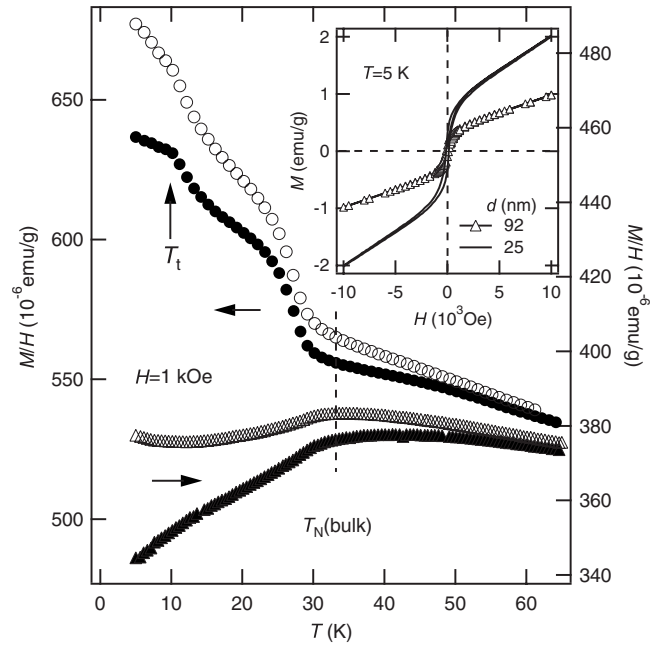


FIG. 2. Magnetic susceptibility, M/H , as a function of temperature at 1 kOe for Co_3O_4 nanocrystals modified by $\text{CH}_3(\text{CH}_2)_8\text{COOH}$ ($d=25$ nm) and $\text{CH}_3(\text{CH}_2)_9\text{NH}_2$ ($d=92$ nm). Open and solid circles (triangles) represent the magnetization-temperature curves after field cooling and zero-field cooling for $d=25$ nm (92 nm), respectively. Inset shows the magnetization of Co_3O_4 nanocrystals modified by $\text{CH}_3(\text{CH}_2)_8\text{COOH}$ and $\text{CH}_3(\text{CH}_2)_9\text{NH}_2$ as a function of magnetic field at $T=5$ K.

creased steeply at the Néel point of bulk samples, $T_N = 32$ K, with decreasing temperature. Additionally, at $T=10$ K an anomalous kink in $\chi(T)$ was also observed, as shown in Fig. 2. As the magnetic field increased, this anomalous point, T_t , shifted toward lower temperatures and disappeared above 30 kOe (Fig. 3). Small thermal hysteresis in the susceptibility was observed above T_t . The ferromagnetic component that developed below T_N also has been observed by Makhlof¹⁴ and Yoshikawa *et al.*¹⁵ for nanoparticles with $d \sim 20$ nm and for nanoscale hollow spheres, respectively. Sato *et al.* reported magnetic properties for diluted systems of Co_3O_4 nanoparticles with diameters of 15–19 nm dispersed into an amorphous silicate matrix.¹⁶⁻¹⁹ In their system, the antiferromagnetic transition disappears and a ferrimagnetism emerges below $T=20$ –30 K.¹⁶⁻¹⁹ Generally, in antiferromagnets, a spontaneous moment emerging below antiferromagnetic transition can be attributed to uncompensated or disordered spins at the surface of nanocrystals.^{2,3} Kodama² claimed that a bilateral spin alignment (composed of two sublattices) is considerably modified and transformed into a multisublattice spin structure because the surface and

TABLE I. Crystallographic and morphological data of the Co_3O_4 nanocrystals.

Modifier	Crystallographic phases	Lattice constant (nm)	Average diameter (TEM) (nm)	Average diameter (XRD) (nm)
$\text{CH}_3(\text{CH}_2)_8\text{COOH}$	Spinel Co_3O_4	0.8100	25	23
$\text{CH}_3(\text{CH}_2)_9\text{NH}_2$	Spinel Co_3O_4	0.8082	92	97

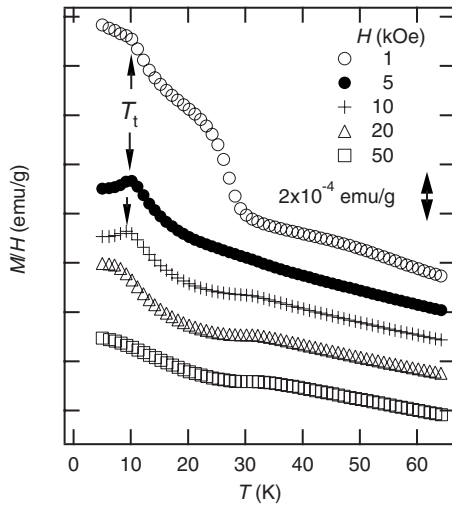


FIG. 3. Magnetic susceptibility, M/H , as a function of temperature at various fields for $d=25$ measured after zero-field cooling. Note that the values of M/H are offset.

core spins become correlated with reducing dimensions of crystals. As shown in Fig. 3, the maximum in $\chi(T) = M(T)/H$ is observed at a higher magnetic field.

In magnetization curves as shown in the inset of Fig. 2, a small ferromagnetic component was detected both in the $\text{CH}_3(\text{CH}_2)_8\text{COOH}$ - and in the $\text{CH}_3(\text{CH}_2)_9\text{NH}_2$ -modified samples. These ferromagnetic components were also observed at room temperature [inset of Fig. 4(a)]. Not only nanocrystalline samples^{14,16–21} but also bulk samples¹⁰ have a small ferromagnetic moment at room temperature. As observed in the bulk sample,¹⁰ the magnetization observed in the present study was linear with increasing magnetic field above $H=3$ kOe, and the magnetization can be extrapolated to a value $M_0(T)$ at zero field. Assuming the typical temperature dependence of M_0 for values above T_N , $M_0(T) = M_0(0)[1 - (T/T_c)^2]^{0.5}$, where T_c is a magnetic transition temperature of the small ferromagnetic component, we estimated M_0 by using the magnetization curves below $H=10$ kOe. Figure 4(b) shows the temperature dependence of M_0 . The fitting parameters were calculated to be $M_0(0) = 0.65$ and 0.38 emu/g and $T_c = 660$ and 630 K for $d=25$ and 92 nm, respectively. Note that T_c obtained is not accurate since the fitted temperature range, $40 < T < 300$ K, is much lower than T_c . As can be seen below, these fitting parameters will be used to estimate the paramagnetic component above T_N . We speculated that this room temperature ferromagnetic component was induced by a configurational deviation from the normal spinel, $(\text{Co}^{2+})[\text{Co}^{3+}_2]\text{O}_4$, to a disordered state, $(\text{Co}^{2+}_{1-\alpha}\text{Co}^{3+}_\alpha)[\text{Co}^{3+}_{2-\alpha}\text{Co}^{2+}_\alpha]\text{O}_4$, where α is the so-called inversion parameter.^{10,22} For a bulk sample, α has been estimated to be 0.0018 from the inverse analog of magnetite for the inverse configuration, $(\text{Co}^{3+})[\text{Co}^{3+}\text{Co}^{2+}]\text{O}_4$,⁸ whereas the crystals synthesized in this work exhibited values of $\alpha = 0.028$ and 0.016 for $d=25$ and 92 nm, respectively. Using high-temperature x-ray powder diffraction, Liu and Prewitt²² observed a continuous transition from normal to disordered spinel at 1150 K in Co_3O_4 with a grain size of less than $1 \mu\text{m}$. The cubic lattice constant, a , in this disordered struc-

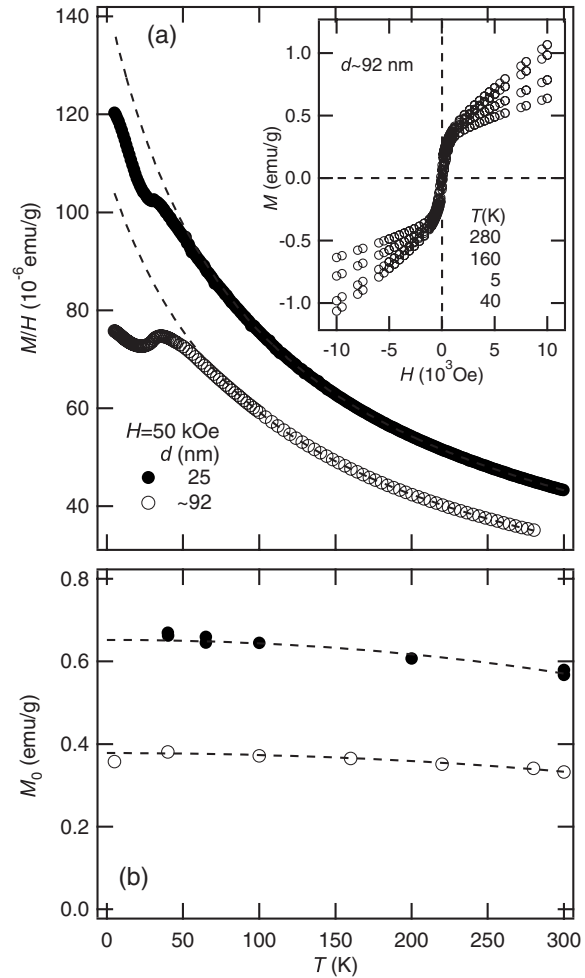


FIG. 4. (a) Magnetic susceptibility, M/H , as a function of temperature measured at 50 kOe for Co_3O_4 nanocrystals modified by $\text{CH}_3(\text{CH}_2)_8\text{COOH}$ and $\text{CH}_3(\text{CH}_2)_9\text{NH}_2$. Inset shows magnetization of Co_3O_4 nanocrystals modified by $\text{CH}_3(\text{CH}_2)_9\text{NH}_2$ as a function of magnetic field at $T=5, 40, 160,$ and 300 K. Dashed lines represent curves calculated from the Curie-Weiss law with a small ferromagnetic correction, $M_0(T)$. (b) Small ferromagnetic components of $M_0(T)$ for $d=25$ and 92 nm obtained from the magnetization-field curves below $H=10$ kOe. Dashed curves are the fitting curves (see text).

ture is larger than that observed in a normal structure, whereas the oxygen parameter, u , decreases above the transition. Although this lattice expansion was observed in the $\text{CH}_3(\text{CH}_2)_8\text{COOH}$ -modified sample, we could not verify that α increased with decreasing crystal size because, possibly, the oxidation state of Co_3O_4 nanocrystals changed with decreasing crystal size, as has been observed in CeO_2 nanocrystals smaller than 10 nm.^{23,24} The electronic state of Ce ion deviates from that of a bulk of CeO_2 due to oxygen vacancies created at the surface.²⁴

Assuming the typical temperature dependence of M_0 , $M_0(T) = M_0(0)[1 - (T/T_c)^2]^{0.5}$ as mentioned above, we estimated the paramagnetic component $\chi(T)$ at $H=50$ kOe. $\chi(T)$ obeys the Curie-Weiss law, $\chi = \chi_0 + [C/(T - \theta)]$, where χ_0 , C , and θ are the constant susceptibility, the Curie constant, and the Weiss temperature, respectively. Figure 4

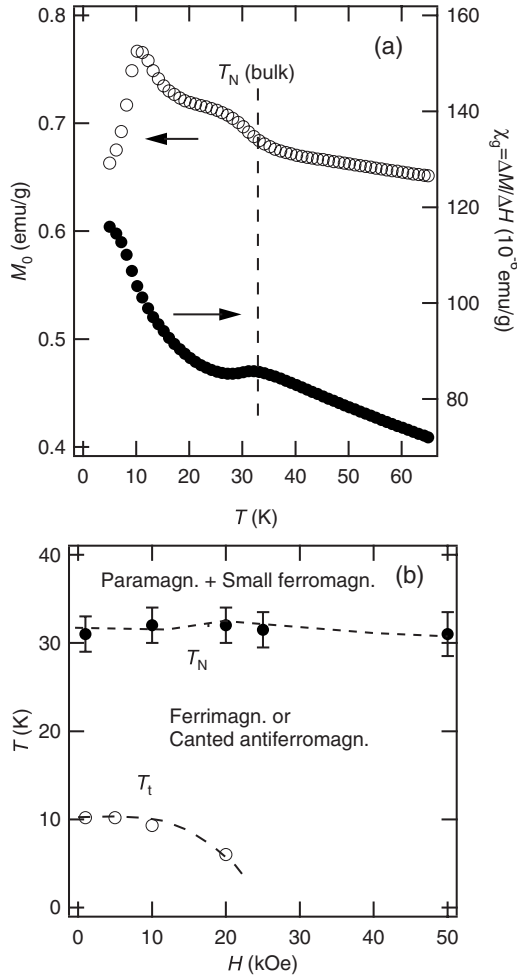


FIG. 5. (a) Ferromagnetic moment, M_0 , and differential susceptibility, $\Delta M/\Delta H$, for $d \sim 25$ nm as a function of temperature obtained in $5 < H < 20$ kOe. (b) Proposed temperature–magnetic field phase diagram of Co_3O_4 nanoparticles with 25 nm diameter.

shows $M(T)/H$ at $H=50$ kOe with the least-squares fitting curves for $d=25$ and 92 nm. For $d=25$ nm, χ_0 , the effective magnetic moment per Co ion, p_{eff} , and θ were estimated to be 1.7×10^{-4} emu/mol $_{\text{Co}}$, $2.72\mu_B$, and -90 K, respectively. For $d=92$ nm, $\chi_0=1.0 \times 10^{-4}$ emu/mol $_{\text{Co}}$, $p_{\text{eff}}=2.53\mu_B$, and $\theta=-102$ K; these values are comparable to those obtained for a bulk sample of Co_3O_4 .¹⁴ In these estimations, the inversion in the spinel structure was ignored because the inversion parameters were less than 0.03. However, the effective magnetic moment for $d=25$ nm was substantially larger than those for $d=92$ nm ($2.53\mu_B$) and for a bulk sample ($2.54\mu_B$).²⁵

To distinguish between ferromagnetic and paramagnetic components from the magnetization data near the transitions at T_N and T_i , we tried to fit $M(T, H)$ to the equation of $M(T, H)=M_0(T)+\chi(T)H$. Figure 5(a) shows the temperature dependence of M_0 and χ obtained in the ranges of $5 < H < 20$ kOe. At $T \sim 32$ K, $\chi(T)$ exhibited an obvious maximum, whereas below 32 K an increase in $\chi(T)$ was observed. The ferromagnetic component, M_0 , increased steeply at the point at which χ exhibited a maximum, then dropped suddenly at T_i . Figure 5(b) shows a temperature–magnetic field

phase diagram proposed in this study. As shown in Fig. 5(b), the T_i - H curve shows a field dependence, $T_i(H)=T_i(0)[1-(H/H_0)^2]^\beta$, with $\beta \sim 0.6$, $H_0 \sim 27$ kOe, and $T_i(0) \sim 10$ K. This low temperature anomaly is possibly comparable to an anomaly observed for a diluted Co_3O_4 nanoparticles embedded on a silica matrix^{16–19} since below T_i the difference between $M(T)$ curves measured after zero-field cooling (ZFC) and field cooling (FC) increased substantially. Comparison with bulk CoAl_2O_4 ,^{26–28} which has the same magnetic state of Co^{2+} at the A site ($S=3/2$), the hysteresis below T_i can be plausibly attributed to the spin-glass-like state, whereas, on the other hand, in a canonical spin glass a cusp at a freezing temperature in $\chi(T)$ is swept out at lower magnetic field. The demagnetization below T_i suggests that the ordered magnetic spins are reoriented or frozen randomly (spin glass). As crystal size decreases, the antiferromagnetism splits into a ferrimagnetic and a spin-glass (SG) states. In contrast, in bulk CoAl_2O_4 the spin-glass state appears instead of an antiferromagnetic transition, whereas the glass transition temperature depends strongly on the inversion parameter α .²⁸

Finally, we discuss the magnetic structure of the Co_3O_4 crystals with $d=25$ nm, assuming a finite spin at the B site detected in the paramagnetic region, $T > T_N$. As mentioned above, p_{eff} for $d=25$ nm estimated for $100 < T < 300$ K is substantially larger than that for $d \sim 92$ nm. Also, p_{eff} is calculated to be $2.24\mu_B/\text{Co}$ ion with the free spin g factor $g=2$ and $S=3/2$ and 0 at the A and B sites, respectively.^{10,11} However, as indicated in this and previous studies,¹⁴ p_{eff} is larger than the estimated value, $p_{\text{eff}}=(2.5-2.72)\mu_B$, for nanocrystal samples with $d=16-25$ nm. Because the lattice volume for $d=25$ nm expanded 0.7% compared with the volumes for $d \sim 92$ nm and the bulk (Table I), it is plausible that the crystal field splitting decreased and the low-spin state was hybridized with the high spin state for the Co^{3+} state at the B site. Expectedly, a so-called intermediate spin state having a finite spin of $S > 0$ at the B site has been established.²⁹ These spins bring about significant effects on the antiferromagnetism of Co_3O_4 nanocrystals by superexchange interactions via $\text{Co}^{2+}(\text{A})-\text{O}-\text{Co}^{2+}(\text{B})-\text{O}-\text{Co}^{2+}(\text{A})$. Another scenario is related to the valence transformation observed in ceria nanocrystals. The lattice of ceria nanocrystals, $\text{CeO}_{2-\delta}$, expands significantly below $d \sim 10$ nm, with a valence transformation from Ce^{4+} to Ce^{3+} .^{23,24} In the case of Co_3O_4 nanocrystals, we cannot rule out that the valence state transformed from Co^{3+} to Co^{2+} at the B sites; consequently, an induced finite spin $S > 0$ at the B sites can modify the antiferromagnetic spin structure at the A sites. Therefore, we can suggest that the rising of spontaneous moment below T_N observed in the nanocrystal with $d=25$ nm reveals a ferrimagnetic or a canted antiferromagnetic ordering that magnetic moments on the magnetic sublattices do not cancel out completely. Further investigations are needed to clarify the spin structures and electronic states below and above the magnetic transitions.

IV. CONCLUSION

In conclusion, cobalt oxide spinel Co_3O_4 nanocrystals were produced by hydrothermal synthesis with average di-

ameters of 25 and 92 nm. The smaller nanocrystals exhibited magnetic anomalies at the Néel point, $T_N=32$ K, and at $T_f \sim 10$ K, whereas the larger crystals displayed a maximum in magnetization at T_N that was similar to that observed for bulk Co_3O_4 samples. Maximum spontaneous magnetization was observed at T_f ; above $H \sim 30$ kOe this anomaly vanished. The ferromagnetic component increased rapidly at the point of maximum susceptibility (i.e., at the Néel point). This observation, along with the contrast in results between the smaller and larger particle samples, leads us to conclude that the spontaneous moment appeared because the antiferromag-

netic ground state was modified when the particle diameter approached 20–30 nm. From the results of this study, a temperature–magnetic field phase diagram was obtained up to 50 kOe.

ACKNOWLEDGMENTS

This research was partly supported by a Grant-in-Aid for the COE project, Giant Molecules and Complex Systems, 2002 (T.M.), and KAKENHI (Grants No. 19310063 and No. 20226015).

*Corresponding author; FAX: +81 298592701; naka.takashi@nims.go.jp

- ¹G. Srajer, L. H. Lewis, D. D. Bader, A. J. Epstein, C. S. Fadley, E. Fullerton, A. Hoffmann, J. B. Kortright, K. M. Krishnan, S. A. Majetich, T. S. Rahman, C. A. Ross, M. B. Salamon, I. K. Schuller, T. C. Schulthess, and J. Z. Sun, *J. Magn. Magn. Mater.* **307**, 1 (2006).
- ²R. H. Kodama, *J. Magn. Magn. Mater.* **200**, 359 (1999); Q. A. Pankhurst, J. Connolly, S. K. Jones, and J. Dobson, *J. Phys. D* **36**, R167 (2003).
- ³L. Néel, in *Low Temperature Physics*, edited by B. Dewitt, B. Dreyfus, and P. D. de Gennes (Gordon and Beach, New York, 1962).
- ⁴T. Mousavand, S. Takami, M. Umetsu, S. Ohara, and T. Adschiri, *J. Mater. Sci.* **41**, 1445 (2006).
- ⁵J. Zhang, S. Ohara, M. Umetsu, T. Naka, Y. Hatakeyama, and T. Adschiri, *Adv. Mater. (Weinheim, Ger.)* **19**, 203 (2007).
- ⁶T. Mousavand, S. Ohara, M. Umetsu, J. Zhang, S. Takami, T. Naka, and T. Adschiri, *J. Supercrit. Fluids* **40**, 397 (2007).
- ⁷T. Mousavand, J. Zhang, S. Ohara, M. Umetsu, T. Naka, and T. Adschiri, *J. Nanopart. Res.* **9**, 1067 (2007).
- ⁸K. Hayashi, H. Morii, K. Iwasaki, S. Horie, N. Horiishi, and K. Ichimura, *J. Mater. Chem.* **17**, 527 (2007).
- ⁹H. Althues, P. Simon, F. Philipp, and S. Kaskel, *J. Nanosci. Nanotechnol.* **6**, 409 (2006).
- ¹⁰W. L. Roth, *J. Phys. Chem. Solids* **25**, 1 (1964).
- ¹¹C. D. Spencer and D. Schroer, *Phys. Rev. B* **9**, 3658 (1974).
- ¹²C. L. Dong, C. L. Chen, K. Asokan, Y. Y. Chen, P. C. Chen, Y. S. Liu, J. L. Chen, C. L. Chang, H. J. Lin, J. F. Lee, and J.-H. Guo, *Phys. Status Solidi B* **244**, 4526 (2007).
- ¹³JCPDS Card No. 42-1467.
- ¹⁴S. A. Makhlof, *J. Magn. Magn. Mater.* **246**, 184 (2002).
- ¹⁵H. Yoshikawa, K. Hayashida, Y. Kozuka, A. Horiguchi, K. Agawa, S. Bandow, and S. Iijima, *Appl. Phys. Lett.* **85**, 5287 (2004).
- ¹⁶Y. Hayakawa, S. Kohiki, M. Sato, Y. Sonda, T. Babasaki, H. Deguchi, A. Hidaka, H. Shimooka, and S. Takahashi, *Physica E (Amsterdam)* **9**, 250 (2001).
- ¹⁷M. Sato, S. Kohiki, Y. Hayakawa, Y. Sonda, T. Babasaki, H. Deguchi, and M. Mitome, *J. Appl. Phys.* **88**, 2771 (2000).
- ¹⁸Y. Ichiyanagi, Y. Kimishima, and S. Yamada, *J. Magn. Magn. Mater.* **272-276**, E1245 (2004).
- ¹⁹S. Takada, M. Fujii, S. Kohiki, T. Babasaki, H. Deguchi, M. Mitome, and M. Oku, *Nano Lett.* **1**, 379 (2001).
- ²⁰S. R. Ahmed and P. Kofinas, *J. Magn. Magn. Mater.* **288**, 219 (2005).
- ²¹J. Jiang and L. Li, *Mater. Lett.* **61**, 4894 (2007).
- ²²X. Liu and C. T. Prewitt, *Phys. Chem. Miner.* **17**, 168 (1990).
- ²³S. Tsunekawa, K. Ishikawa, Z. Q. Li, Y. Kawazoe, and A. Katsuya, *Phys. Rev. Lett.* **85**, 3440 (2000).
- ²⁴S. Tsunekwa, S. Ito, and Y. Kawazoe, *Appl. Phys. Lett.* **85**, 3845 (2004).
- ²⁵This value, $2.54\mu_B$, was estimated by using the susceptibility reported in Ref. 10 in the same temperature range of $100 < T < 300$ K.
- ²⁶N. G. Matveeva and A. I. Shelykh, *Phys. Status Solidi B* **50**, 83 (1972).
- ²⁷T. Suzuki, H. Nagai, M. Nohara, and H. Takagi, *J. Phys.: Condens. Matter* **19**, 145265 (2007).
- ²⁸N. Tristan, J. Hemberger, A. Krimmel, H. A. Krug von Nidda, V. Tsurkan, and A. Loidl, *Phys. Rev. B* **72**, 174404 (2005).
- ²⁹K. Asai, O. Yokokura, M. Suzuki, T. Naka, T. Matsumoto, H. Takahashi, N. Mori, and K. Kohn, *J. Phys. Soc. Jpn.* **66**, 967 (1997).